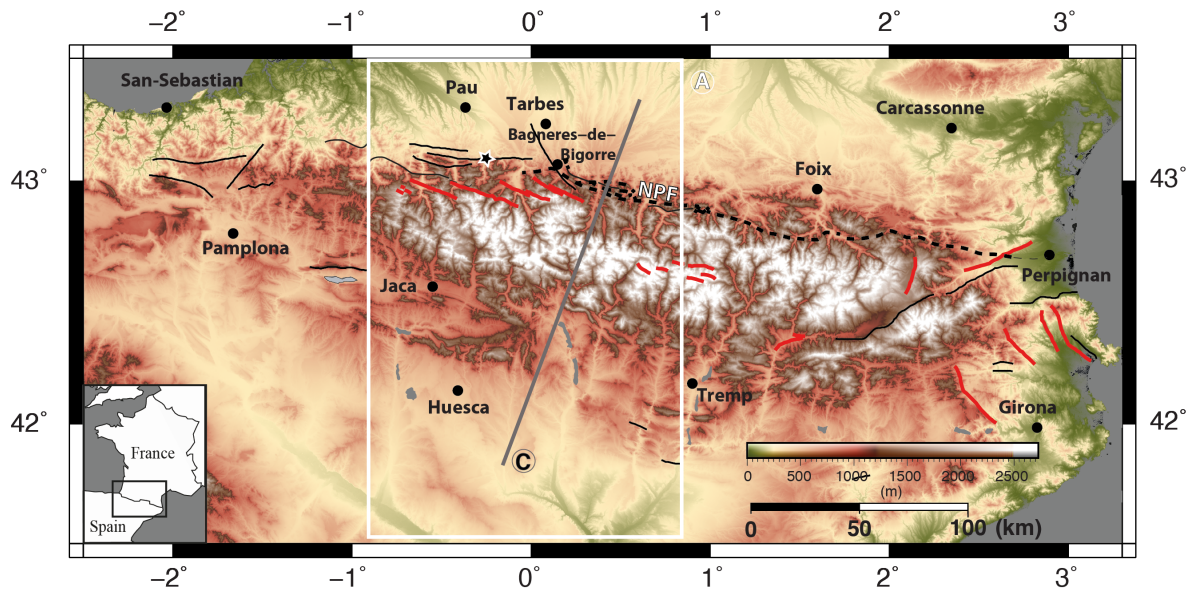
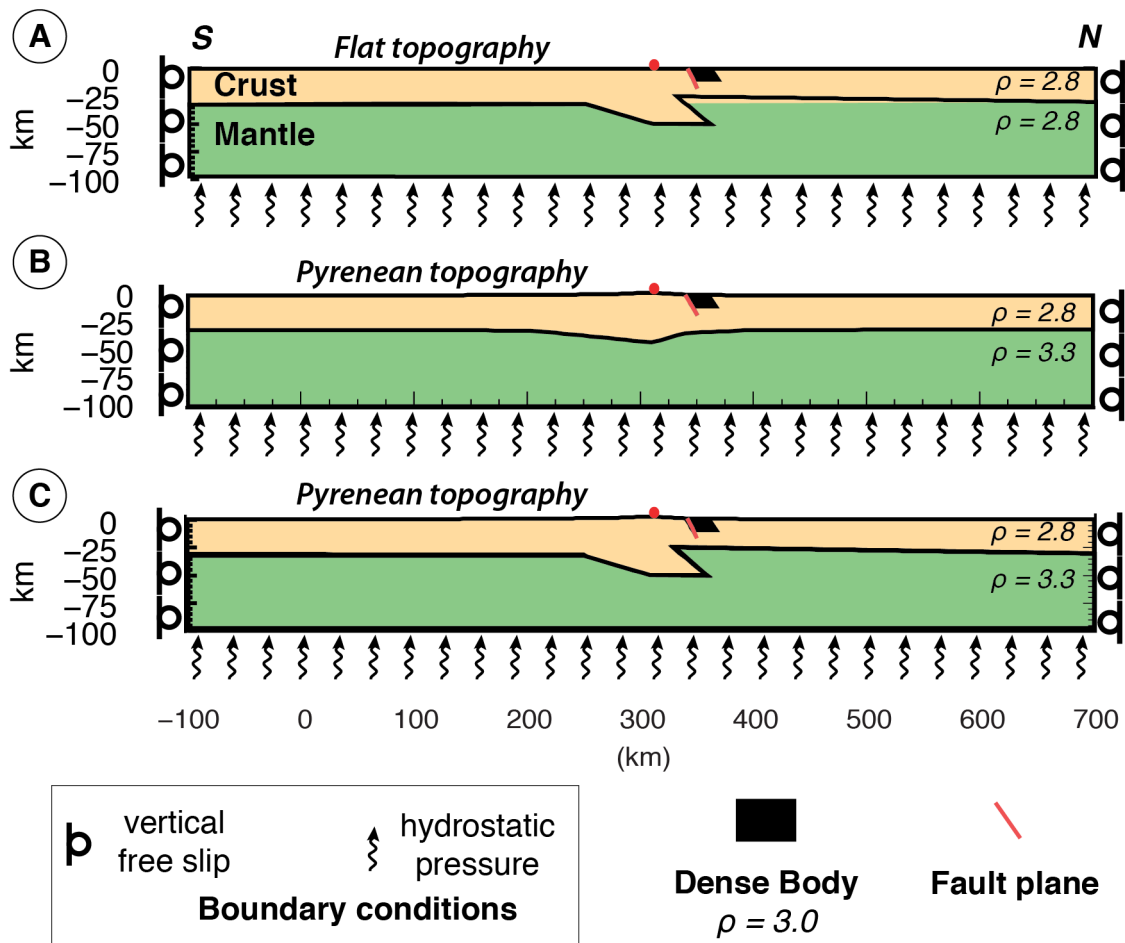


1 Electronic supplement



2
3 **Figure 1.bis :**
4 Topographic map of the Pyrenees. Solid lines are for faults with evidence of post-
5 orogenic activity and red lines highlight normal faults (from Lacan & Ortuno, 2012). The
6 dashed line is for the North Pyrenean Fault (NPF) which is not reported as an active
7 fault. White box gives the location of figure 1A.
8

9 **Three models geometry and their boundary conditions:**



10
11
12
13
14
15
16
17
18
19
20

Figure 2.bis: model setting:

(A) Flat Topography model (**FLAT**) with the same density for the crust and mantle, (B) Isostatic Pyrenean Model (**ISO**), the moho depth locally compensates the topography, and (C) Pyrenean Model (**PYR**) based on Fig. 1D. Horizontal boundary conditions are set to 0 mm/yr but vertical motions are allowed, hydrostatic pressure is applied at the base of the model. The red point is the reference mark shown in Figure 1 and used to extract the evolution of the position versus time in Fig. 3.

21 **Rheological layering**

22 We divide the lithosphere in two layers: the crustal and the upper mantle (Fig.
23 2.bis A-C). We use seismologically derived parameters to model the elastic deformation
24 (Table 1). Beyond the elastic limit, we assume that the anelastic stress-strain relations in
25 the lithosphere are controlled by frictional and viscous processes (Brace and Kohlstedt
26 1980). Therefore, we use the same generic elasto-plastic-viscous rheology for the crust
27 and the mantle. Average values of rheological parameters for the continental lithosphere
28 are used (Table 1). At low temperature, activation of frictional processes is modelled by

29 a Drucker-Prager flow law with an internal friction angle of 15°. In this case, the limit
 30 stress of the medium is mostly dependent from the average stress. Non-linear viscous
 31 relation is assumed at higher temperature using experimentally derived parameters for
 32 quartz-rich rock (crust) and olivine rich-rocks (mantle). Following the concept of stress
 33 envelope (Brace and Kohlstedt, 1980), we choose among viscoelastic and elastic
 34 frictional behaviors considering that the rheology with the minimum deviatoric stress
 35 invariant controls the deformation process (Chery et al. 2001). According to this dual
 36 behavior, our rheological model naturally reflects parameter variations such as strain-
 37 rate, stress and temperature.

38 In order to mimic the localized strain associated with crustal faulting, we also use
 39 material discontinuities with a frictional criterion inside the crust. This makes possible
 40 to explore the consequences of inherited fault weakness on the present-day strain.

41

Parameters and units	Crust (quartz-rich)	Mantle (olivine-rich)
ρ , kg.m ⁻³	2800	3300
E, GPa	10	10
ν	0.25	0.25
c, MPa	10	10
f	15	15
g_0 , Pa ⁿ .s ⁻¹	6.03 10 ⁻²⁴	7.0 10 ⁻¹⁴
n	2.72	3.0
Ea, kJ.mol ⁻¹	134	510

42 Table 2. Parameters values used for crustal and mantle materials. These parameters are
 43 density (ρ), Young modulus (E), Poisson ratio (ν), cohesion (c), internal friction angle (f),
 44 pre-exponential term of the power law (g_0), exponent of the power law (n), activation
 45 energy (Ea).

46

47 **Temperature field**

48 Because of the strong dependence of rheology with temperature, the definition of
 49 the temperature field of the model has a large impact on the model deformation (Kirby
 50 1987). Unfortunately, surface heat flow measurements in mountainous areas weakly
 51 reflect conductive processes occurring in the lithosphere. Indeed, meteoritic water

52 circulation associated with topography largely alters heat transport (Cabal and
53 Fernández 1995) as attested by hydrothermal features of the north Pyrenean zone (e.g.
54 Levet et al., 2002). We therefore define a temperature model for the Pyrenees based on
55 simple considerations. We choose a temperature field outside of the Pyrenees associated
56 with a surface heat flow of 60 mW/m^2 , a radiogenic heat production of 1 mW/m^3 in the
57 crust and a mantle heat flow of 15 mW/m^2 . These parameters are roughly consistent
58 with the heat flow knowledge in the Pyrenean surroundings (Lucazeau and Vasseur
59 1989) and lead to a Moho temperature of 650°C . Because of the lack of reliable
60 conductive heat flow data in the Pyrenees, we simply assume that the radiogenic heat
61 production in the thickened Pyrenean crust should lead to a surface heat flow of 80
62 mW/m^2 . We model the heat flow anomaly of the Pyrenean root by imposing a thermal
63 anomaly located in the crustal root (Fig. 2D). This leads to a temperature of 650°C at 30
64 km depth in the foreland and 1000°C at the root bottom in central part of the range.

65

66 **Boundary conditions**

67 The lack of detectable horizontal motions in western Europe (Nocquet 2012)
68 forces us to set the differential velocity across the profile to zero. However, we do not
69 prescribe the vertical motion on the lateral sides of the model for allowing a possible
70 flexural response of the foreland. All models are supported at their bottom by
71 hydrostatic pressure representing the interaction with an asthenosphere having a
72 density of mantle. Because of these boundary conditions, deformation should occur only
73 in response from body forces and surface processes.

74

75 **Initial conditions and time-stepping**

76 The problem of initial conditions of a geodynamical model is mostly associated
77 with the lack of knowledge of the initial stress state and geometry. In a simple
78 configuration associated with horizontal layering and no lateral density variation, it is
79 possible to compute a lithostatic stress field that exactly balances body forces and
80 boundary conditions. This is the case of FLAT experiments that are in a perfect self-
81 equilibrium. For ISO and PYR experiments, lateral density contrast induces transient
82 motions allowing for the deviatoric stress to build up. We experimentally observe that a
83 period of time of 2Ma and 20Ma are necessary to obtain a nearly complete strain
84 relaxation for respectively ISO and PYR experiments. Therefore, FLAT and ISO

85 experiments are conducted during 2Ma without imposing additional loading. For PYR
86 experiments this time is extended to 20 Ma. After this initial stress building, additional
87 loading (dense body and/or surface processes) is applied during 1 Ma and the friction
88 fault is reduced to 0.02.

89

90 References:

- 91 Brace, W.F., Kohlstedt, D.L., 1980. Limits on Lithospheric Stress Imposed by Laboratory Experiments. *J.*
92 *Geophys. Res.* 85: 6248–6252.
- 93 Cabal, J., Fernández, M., 1995. Heat Flow and Regional Uplift at the North-Eastern Border of the Ebro
94 Basin, NE Spain. *Geophys. J. Int.* 121: 393–403.
- 95 Chery, J., Zoback, M.D., Hassani, R., 2001. An Integrated Mechanical Model of the San Andreas Fault in
96 Central and Northern California., *J. Geophys. Res.* 106, 22051-22066.
- 97 Kirby, S.H., Kronenberg, A.K., 1987. Rheology of the Lithosphere: Selected Topics. *Rev. Geophys.* 25: 1219–
98 1244.
- 99 Levet, S., Toutain, J.P., Munoz, M., Berger, G., Négrel, P., 2002. Geochemistry of the Bagnères-De-Bigorre
100 Thermal Waters From the North Pyrenean Zone (France). *Geofluids.* (2) 25-40.
- 101 Lucazeau, F., Vasseur, G., 1989. Heat-Flow Density Data From France and Surrounding Margins.
102 *Tectonophysics* 164 (2-4): 251–258.
- 103 Nocquet, J.M., 2012. Present-day kinematics of the Mediterranean: a comprehensive overview of GPS
104 results. *Tectonophysics*, April. 1–75. doi:10.1016/j.tecto.2012.03.037.
- 105